

Rapidity dependence of global polarization in heavy ion collisions*

Zuo-Tang Liang(梁作堂)^{1†} Jun Song(宋军)^{2‡} Isaac Upsal^{3§} Qun Wang(王群)^{4¶} Zhangbu Xu(许长补)^{3‡}

¹Institute of Frontier and Interdisciplinary Science, Key Laboratory of Particle Physics and Particle Irradiation (MOE), Shandong University, Qingdao 266237, China

²Department of Physics, Jining University, Shandong 273155, China

³Physics Department, Brookhaven National Laboratory, Upton, New York 11973, USA

⁴Department of Modern Physics, University of Science and Technology of China, Hefei 230026, China

Abstract: We use a geometric model for hadron polarization in heavy ion collisions with an emphasis on the rapidity dependence. The model is based on the model of Brodsky, Gunion, and Kuhn, as well as the Bjorken scaling model. We make predictions regarding the rapidity dependence of global Λ polarization in the collision energy range of 7.7-200 GeV by assuming the rapidity dependence of two parameters, κ and $\langle p_T \rangle$. The predictions can be tested by future beam-energy-scan experiments at the Relativistic Heavy Ion Collider of Brookhaven National Lab.

Keywords: polarization, orbital angular momentum, relativistic heavy-ion collisions

DOI: 10.1088/1674-1137/abc065

I. INTRODUCTION

In non-central collisions of heavy ions at high energies, a substantial orbital angular momentum (OAM) is generated. Through spin-orbit couplings in parton-parton scatterings, hadrons can be globally polarized along the OAM of two colliding nuclei [1-3]. In the hydrodynamic picture, the large OAM is distributed into a fluid of quarks and gluons in the form of local vorticity [4-9], which leads to the local polarization of hadrons along the vorticity direction [10, 11] (for a recent review on the subject, see, e.g., [12]).

The global polarization of Λ (including $\bar{\Lambda}$) has been measured in the STAR experiment in Au+Au collisions in the collision energy range of 7.7-200 GeV [13, 14] through their weak decays into pions and protons. The magnitude of the global polarization is approximately a few percent, and it decreases with increasing collision energies. Hydrodynamic and transport models have been proposed to describe the polarization data for Λ from which the vorticity fields can be determined [8, 9, 15-21]. Then, through the integration of the vorticity over the freezeout hyper-surface [10, 11], the global polarization of Λ has been obtained, and it has been found to agree

with the data [20-24].

The previous STAR measurement of the global polarization is limited to the central rapidity region. The behavior of the polarization in the forward rapidity region can shed light on the polarization mechanism. The STAR collaboration is currently working on a series of upgrades in the forward region, which will add calorimetry and charged-particle tracking in the rapidity range [2.5, 4], and it is expected to collect the data of Au+Au collisions at 200 GeV in 2023. Then, Λ and $\bar{\Lambda}$ may be constructed in this forward region, allowing for the measurement of their polarization.

In this paper, we will give a geometric model for the hadron polarization with an emphasis on the rapidity dependence. This work is the natural extension of previous work by some of us [25]. The geometric model is based on the model of Brodsky, Gunion, and Kuhn (BGK) [26] as well as the Bjorken scaling model [25, 27]. The BGK model can provide a good description of the hadron's rapidity distribution in nucleus-nucleus collisions.

The rest of this paper is organized as follows. In Sec. II, we give formulas for the average longitudinal momentum and local orbital angular momentum using the method of Ref. [25], where the rapidity distribution of

Received 16 June 2020; Accepted 24 July 2020; Published online 15 October 2020

* ZTL and QW are supported in part by the National Natural Science Foundation of China (NSFC) (11890713, 11535012). JS is supported in part by Shandong Province Natural Science Foundation (ZR2019YQ06)

[†]E-mail: liang@sdu.edu.cn

[‡]E-mail: songjun2011@jnxu.edu.cn

[§]E-mail: iupsalp@gmail.com

[¶]E-mail: qunwang@ustc.edu.cn

[‡]E-mail: xzb@bnl.gov

©2021 Chinese Physical Society and the Institute of High Energy Physics of the Chinese Academy of Sciences and the Institute of Modern Physics of the Chinese Academy of Sciences and IOP Publishing Ltd

hadrons is given by the BGK model. In Sec. III, we use the hard sphere and Woods-Saxon model [28] for the nuclear density distribution to calculate the rapidity distribution of hadrons. In Sec. IV, the hadron polarization from the local OAM is calculated with the WS nuclear density distribution. By constraining the parameter using the polarization data at mid-rapidity, we make predictions of the polarization in the forward rapidity region. A summary is given in the final section.

II. AVERAGE LONGITUDINAL MOMENTUM AND LOCAL ORBITAL ANGULAR MOMENTUM

There is an intrinsic rotation of the initially produced matter in the reaction plane in non-central heavy ion collisions. The rotation can be characterized by a tilted local rapidity distribution of produced hadrons toward the projectile and target direction in the transverse plane. We consider non-central collisions of two nuclei $A+A$: the first one is regarded as the projectile moving in the z direction, while the second is regarded as the target moving in the $-z$ direction; see Fig. 1 for an illustration. The impact parameter is in the direction from the target to the projectile, i.e., in the x direction. The orbital angular momentum (OAM) is in the direction determined by the vector product of the impact parameter and the projectile momentum, $\mathbf{b} \times \mathbf{p}_{\text{proj}}$ which is the $-y$ direction.

In the center of the rapidity frame for $p+A$ collisions, the proton has rapidity Y_L and interacts at a transverse impact parameter \mathbf{r}_T with $N_{\text{part}}^A \approx \sigma_{NN} T_A(\mathbf{r}_T)$ nucleons with rapidity $-Y_L$, where $T_A(\mathbf{r}_T)$ is the thickness function or the number of nucleons per unit area

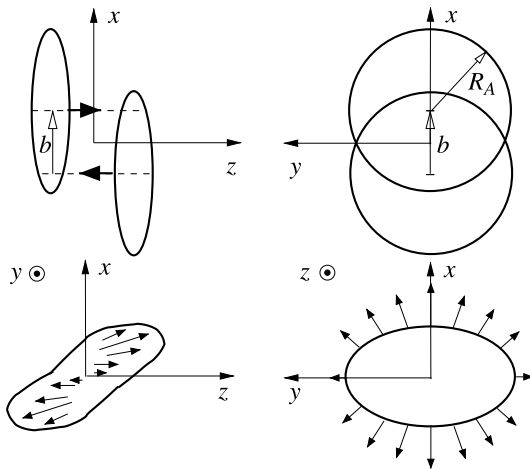


Fig. 1. Schematic figure taken from [25] for non-central heavy ion collisions with impact parameter \mathbf{b} pointing in the x direction. The orbital angular momentum is in the $-y$ direction.

$$T_A(\mathbf{r}_T) = \int dz \rho_A(\mathbf{r}), \quad (1)$$

where $\mathbf{r} = (x, y, z)$, $\mathbf{r}_T = (x, y)$, and ρ_A is the number density of nucleons in the nucleus, σ_{NN} is the inelastic cross-section of nucleon-nucleon collisions, and $Y_L \approx \ln[\sqrt{s}/(2m_N)]$ is the largest rapidity. The triangular rapidity distribution of hadrons is the result of string fragmentation between the projectile proton and the target nucleus. The hadrons produced by the wounded projectile proton are in the rapidity range $Y \in [0, Y_L]$, while those produced by the wounded target nucleons are in the range $Y \in [-Y_L, 0]$. The rapidity distribution of produced hadrons is approximately given by the BGK model [26] as

$$\frac{d^3 N_{pA}}{d^2 \mathbf{r}_T dY} = \frac{dN_{pp}}{dY} \left[T_A(\mathbf{r}_T) \frac{Y_L - Y}{2Y_L} + T_p \frac{Y_L + Y}{2Y_L} \right], \quad (2)$$

where $T_p \approx 1$ is the number of projectile protons per unit area. In the forward or projectile region $Y \approx Y_L$, the rapidity distribution approaches that of $p+p$ collisions dN_{pp}/dY , while in the backward or target region, it approaches $(dN_{pp}/dY)T_A(\mathbf{r}_T)$. From the experimental data, we take a Gaussian form for dN_{pp}/dY ,

$$\frac{dN_{pp}}{dY} = a_1 \exp\left(-\frac{Y^2}{a_2}\right) \frac{1}{\sqrt{1 + a_3(\cosh Y)^4}}, \quad (3)$$

where a_1 , a_2 , and a_3 are parameters: a_1 sets the magnitude at $Y = 0$, and a_2 and a_3 describe the width of the rapidity distribution. The values of these parameters in inelastic non-diffractive events for $p+p$ collisions are determined by simulation results using PYTHIA8.2 [29] (see Fig. 2) and are listed in Table 1.

The trapezoidal shape of the rapidity distribution in (2) in the BGK model is a consequence of the string frag-

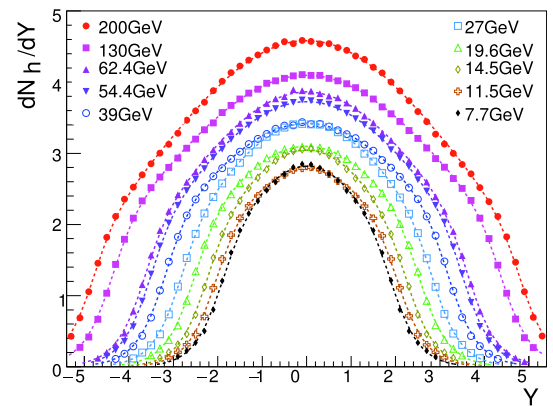


Fig. 2. (color online) Simulation results of hadron rapidity distributions in inelastic non-diffractive events for $p+p$ collisions using PYTHIA8.2. The curves of Eq. (3) are shown in lines.

Table 1. Values of parameters in the hadron rapidity distribution in inelastic non-diffractive events for $p+p$ collisions at various collision energies from simulation using PYTHIA8.2 [29].

| $\sqrt{s_{NN}}/\text{GeV}$ | 200 | 130 | 62.4 | 54.4 | 39 | 27 | 19.6 | 14.5 | 11.5 | 7.7 |
|----------------------------|-----------------------|-----------------------|-----------------------|-----------------------|-----------------------|-----------------------|-----------------------|-----------------------|-----------------------|-----------------------|
| a_1 | 4.584 | 4.096 | 3.862 | 3.726 | 3.420 | 3.421 | 3.099 | 3.049 | 2.784 | 2.831 |
| a_2 | 26.112 | 25.896 | 18.911 | 18.931 | 18.779 | 13.555 | 13.629 | 9.947 | 10.488 | 8.008 |
| a_3 | 9.70×10^{-8} | 5.61×10^{-7} | 9.75×10^{-6} | 1.71×10^{-5} | 6.61×10^{-5} | 2.50×10^{-4} | 8.76×10^{-4} | 2.44×10^{-3} | 5.90×10^{-3} | 9.40×10^{-3} |

mentation and can be described naturally using the LUND string [30] and HIJING model [31, 32]. An extension of the BGK model has been applied to the jet tomography of twisted strongly coupled quark-gluon plasmas [33], as well as the global polarization in nucleus-nucleus collisions [4]. In nucleus-nucleus collisions with projectile A and target B , at the point $\mathbf{r}_T = (x, y)$ in the transverse plane in the participant region (the coordinate system is shown in the upper-left of Fig. 1), the rapidity distribution of produced hadrons has the form that is a generalization of Eq. (2), i.e., the sum over contributions from projectile ('proj') and target ('tar')

$$\begin{aligned} \frac{d^3 N_{AB}}{d^2 \mathbf{r}_T dY} &= \frac{d^3 N_A^{\text{proj}}}{d^2 \mathbf{r}_T dY} + \frac{d^3 N_B^{\text{tar}}}{d^2 \mathbf{r}_T dY} \\ &= \frac{dN_{pp}}{dY} \left[T_A(\mathbf{r}_T - \mathbf{b}/2) \frac{Y_L + Y}{2Y_L} + T_B(\mathbf{r}_T + \mathbf{b}/2) \frac{Y_L - Y}{2Y_L} \right]. \end{aligned} \quad (4)$$

Here, thickness functions $T_A(\mathbf{r}_T - \mathbf{b}/2)$ and $T_B(\mathbf{r}_T + \mathbf{b}/2)$ in Eq. (4) are given by

$$T_{A,B}(\mathbf{r}_T \mp \mathbf{b}/2) = \int dz \rho^{A,B}(\mathbf{r}_T \mp \mathbf{b}/2), \quad (5)$$

where $\rho^{A,B}(\mathbf{r}_T \mp \mathbf{b}/2)$ are the participant nucleon number density functions of nuclei A and B . One can verify that distribution (4) is proportional to $T_{A/B}(\mathbf{r}_T \mp \mathbf{b}/2)$ at $Y = \pm Y_L$.

From Eq. (4), we can derive the distribution in the in-plane position x and the rapidity Y by integrating over the out-plane position y in the range $[-y_m, y_m]$,

$$\begin{aligned} \frac{d^2 N_{AB}}{dx dY} &= \frac{dN_{pp}}{dY} \left\{ \frac{1}{2} \int_{-y_m}^{y_m} dy [T_A(\mathbf{r}_T - \mathbf{b}/2) + T_B(\mathbf{r}_T + \mathbf{b}/2)] \right. \\ &\quad \left. + \frac{Y}{2Y_L} \int_{-y_m}^{y_m} dy [T_A(\mathbf{r}_T - \mathbf{b}/2) - T_B(\mathbf{r}_T + \mathbf{b}/2)] \right\}, \end{aligned} \quad (6)$$

where y_m is the maximum of y at a specific x ; in the hard sphere model of the nuclear density distribution, it is defined by the boundary of the overlapping region of two nuclei, while in the Woods-Saxon model, there is no

sharp boundary, but it can be set to a value much larger than y_m in the hard sphere model. We define the normalized probability distribution of Y at x ,

$$f(Y, x) = \left(\frac{dN_{AB}}{dx} \right)^{-1} \frac{d^2 N_{AB}}{dx dY}, \quad (7)$$

where the distribution dN_{AB}/dx is given by

$$\begin{aligned} \frac{dN_{AB}}{dx} &= \int_{-Y_L}^{Y_L} dY \frac{d^2 N_{AB}}{dx dY} \\ &= \int_0^{Y_L} dY \frac{dN_{pp}}{dY} \int_{-y_m}^{y_m} dy [T_B(\mathbf{r}_T + \mathbf{b}/2) + T_A(\mathbf{r}_T - \mathbf{b}/2)]. \end{aligned} \quad (8)$$

According to the Bjorken scaling model [25], the average rapidity of the particle as a function of Y at x in the rapidity window $[Y - \Delta_Y/2, Y + \Delta_Y/2]$ is given by

$$\langle Y \rangle_\Delta = \frac{\int_{Y-\Delta_Y/2}^{Y+\Delta_Y/2} dY' Y' f(Y', x)}{\int_{Y-\Delta_Y/2}^{Y+\Delta_Y/2} dY' f(Y', x)} \approx Y + \frac{\Delta_Y^2}{12} \frac{1}{f(Y, x)} \frac{df(Y, x)}{dY}, \quad (9)$$

where Δ_Y is the width of the rapidity window in which particles interact to reach collectivity. We assumed $\Delta_Y \ll Y$ so that Δ_Y can be treated as a perturbation. The average rapidity of the particle as a function of x in the full rapidity range reads

$$\begin{aligned} \langle Y \rangle &= \frac{\int_{-Y_L}^{Y_L} dY Y f(Y, x)}{\int_{-Y_L}^{Y_L} dY f(Y, x)} \\ &= \frac{1}{Y_L} \langle Y^2 \rangle_{pp} \frac{\int_{-y_m}^{y_m} dy [T_A(\mathbf{r}_T - \mathbf{b}/2) - T_B(\mathbf{r}_T + \mathbf{b}/2)]}{\int_{-y_m}^{y_m} dy [T_A(\mathbf{r}_T - \mathbf{b}/2) + T_B(\mathbf{r}_T + \mathbf{b}/2)]}, \end{aligned} \quad (10)$$

where $\langle Y^2 \rangle_{pp}$ is defined as

$$\langle Y^2 \rangle_{pp} = \frac{\int_{-Y_L}^{Y_L} dY (dN_{pp}/dY) Y^2}{\int_{-Y_L}^{Y_L} dY (dN_{pp}/dY)}. \quad (11)$$

The average longitudinal momentum p_z and the average energy E_p of the particle are

$$\begin{aligned} \langle p_z \rangle &= \langle p_T \rangle \sinh \langle Y \rangle_\Delta \\ &\approx \langle p_T \rangle \sinh Y + \langle p_T \rangle \frac{\Delta_Y^2}{12} \frac{d \ln f(Y, x)}{dY} \cosh Y, \\ \langle E_p \rangle &= \langle p_T \rangle \cosh \langle Y \rangle_\Delta \\ &\approx \langle p_T \rangle \cosh Y + \langle p_T \rangle \frac{\Delta_Y^2}{12} \frac{d \ln f(Y, x)}{dY} \sinh Y, \end{aligned} \quad (12)$$

where we have treated terms proportional to Δ_Y^2 as a perturbation. At a given Y , we consider two particles located at $x + \Delta x/2$ and $x - \Delta x/2$. In their center of mass frame, the local average OAM for two colliding particles is given by [25]

$$\begin{aligned} \langle L_y \rangle &\approx -(\Delta x) \langle p_z^{\text{cm}} \rangle \\ &\approx -(\Delta x)^2 \langle p_T \rangle \frac{\Delta_Y^2}{24} \frac{d \ln f(Y, x)}{dY dx}, \end{aligned} \quad (13)$$

where $\langle p_z^{\text{cm}} \rangle$ is the average longitudinal momentum in the center of mass frame for one particle. Here, Δx is a typical impact parameter of particle scatterings, and the function $d \ln f(Y, x)/dx dY$ is called the shear of longitudinal momentum (SLM). In the following sections, we will use the average SLM over the in-plane coordinate

$$\left\langle \frac{d \ln f(Y, x)}{dY dx} \right\rangle_x = \frac{\int dx (dN_{AB}/dx dY) (d \ln f(Y, x)/dY dx)}{\int dx (dN_{AB}/dx dY)}, \quad (14)$$

where $dN_{AB}/dx dY$ is given in Eq. (6) as a weight function.

III. RAPIDITY DISTRIBUTIONS OF HADRONS IN HARD SPHERE AND WOODS-SAXON MODELS

In this section, we will calculate the rapidity distributions for hadrons $f(Y, x)$ in Eq. (7) with the hard sphere (HS) and Woods-Saxon (WS) nuclear density distributions, which are involved in the thickness functions in Eq. (5). As a simple illustration, we consider collisions of two identical nuclei with nucleon number A .

A. Hard sphere nuclear density distribution

The HS nuclear density is given by

$$\rho_{\text{HS}}(\mathbf{r}) = \frac{3A}{4\pi R_A^3} \theta(R_A - r), \quad (15)$$

where $R_A = 1.2A^{1/3}$ fm is the radius of the nucleus. The thickness functions have the analytical form

$$T_A(\mathbf{r}_T \pm \mathbf{b}/2) = \frac{6A}{4\pi R_A^3} [R_A^2 - (x \pm b/2)^2 - y^2]^{1/2}. \quad (16)$$

Inserting the above into Eq. (4), we obtain the hadron distribution $dN_{AA}/(dx dy dY)$, whose numerical results are shown in Fig. 3 at three rapidity values in Au+Au collisions at $\sqrt{s_{NN}} = 200$ GeV with the impact parameter $b = 1.2R_A$. In the HS model, the overlapping region of two

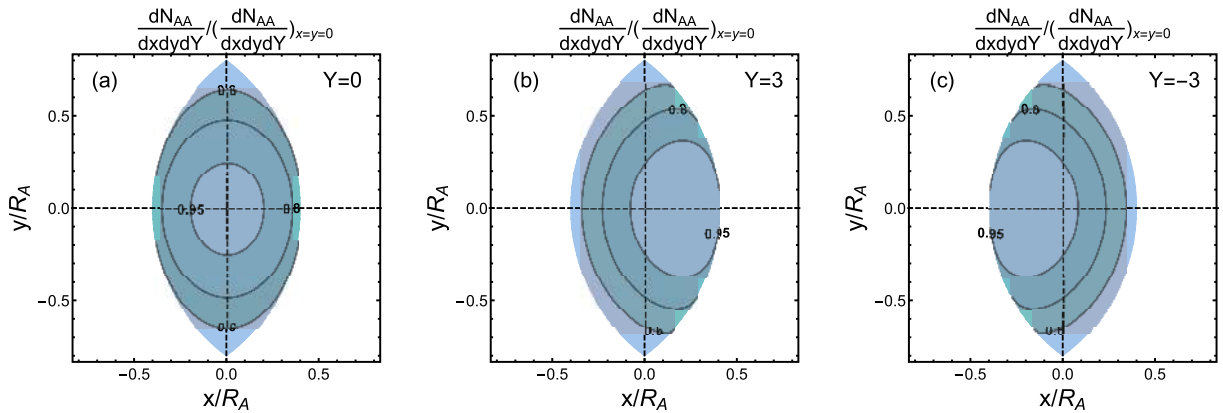


Fig. 3. (color online) Hadron distributions (contour plot) in the HS model in the transverse plane for Au+Au collisions at $\sqrt{s_{NN}} = 200$ GeV and $b = 1.2R_A$. The number on the contour line denotes the value on the line normalized by that at the origin. The rapidity values are chosen to be (a) $Y = 0$ (central), (b) $Y = 3$ (forward), and (c) $Y = -3$ (backward).

nuclei is limited by $|x| < R_A - b/2$ and $|y| < \sqrt{R_A^2 - (|x| + b/2)^2}$. We see that the distribution at $Y = 0$ is symmetric in x and y , while the distribution in the forward (backward) rapidity is shifted to the right (left) in the x direction.

Integrating over the out-plane coordinate y , we obtain the hadron distribution function

$$\frac{d^2 N_{AA}}{dx dY} = \frac{6A}{4\pi R_A^3} \frac{dN_{pp}}{dY} \left[C_1^+ + C_1^- + \frac{Y}{Y_L} (C_1^+ - C_1^-) \right], \quad (17)$$

where C_1^\pm are defined in Eq. (27). In Fig. 4(a), we show $dN_{AA}/dx dY$ as functions of the in-plane coordinate x at various rapidity values. We see that the distribution at $Y = 0$ is symmetric, while the distribution at forward (backward) rapidity is shifted to the positive (negative) x . The magnitude of the shift increases slightly with the rapidity. In Fig. 4(b), we show $dN_{AA}/dx dY$ as functions of the rapidity Y for various values of x . We see that the distribution at $x = 0$ is symmetric, while that at positive (negative) x is tilted to the forward (backward) rapidity. From Eq. (7), we obtain the normalized function $f(Y, x)$ as

$$f(Y, x) = \frac{dN_{pp}/dY}{2 \int_0^{Y_L} dY (dN_{pp}/dY)} \left(1 + \frac{Y}{Y_L} \cdot \frac{C_1^+ - C_1^-}{C_1^+ + C_1^-} \right), \quad (18)$$

where $|x| \leq R_A - b/2$ and $b \leq 2R_A$. The numerical results of $f(Y, x)$ are shown in Fig. 4(c, d).

The derivative of $\ln f(Y, x)$ with respect to Y and x is derived in Eq. (37), from which one can obtain the average SLM through Eq. (14). We show numerical results of the average SLM in Fig. 5 as rapidity functions in Au+Au collisions at various collision energies. The average SLM increases slowly with the rapidity via the Y/Y_L term, which can be seen in Eq. (37). The energy dependence of the average SLM is mostly controlled by $Y_L \approx \ln[\sqrt{s}/(2m_N)]$, as shown in Eq. (37). The relatively obvious increase in the forward rapidity region is an artifact of the HS model in comparison with the WS model in the next subsection. The reason for this is that there is a sharp decrease in the nucleon density at the nucleus boundary in the HS model, which gives an infinite derivative in the SLM in the forward rapidity region. In the WS model, however, the decrease in the nucleon density at the boundary is smooth, resulting in a mild increase in the av-

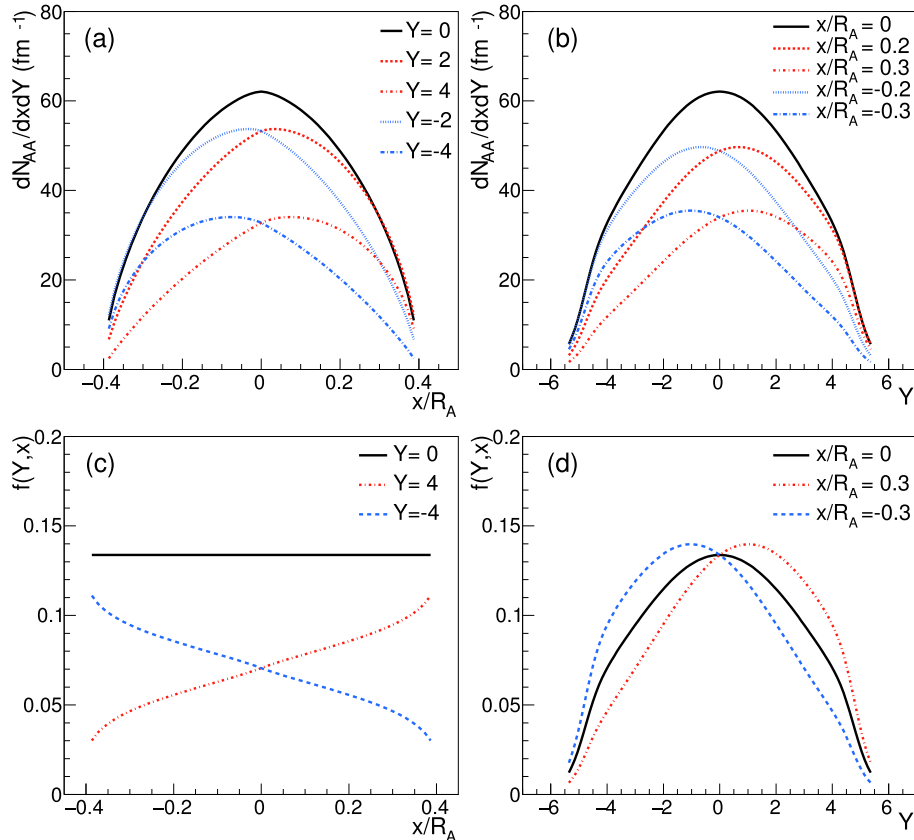


Fig. 4. (color online) Hadron distributions in the HS model in Au+Au collisions at $\sqrt{s_{NN}} = 200$ GeV as functions of (a) the in-plane position x at different rapidity values and as functions of (b) the rapidity Y at different values of x . The impact parameter is set to $b = 1.2R_A$. (c) The normalized distribution $f(Y, x)$ as functions of x at different Y . (d) The normalized distribution $f(Y, x)$ corresponding to (b). The definition of $f(Y, x)$ is given in Eq. (18).

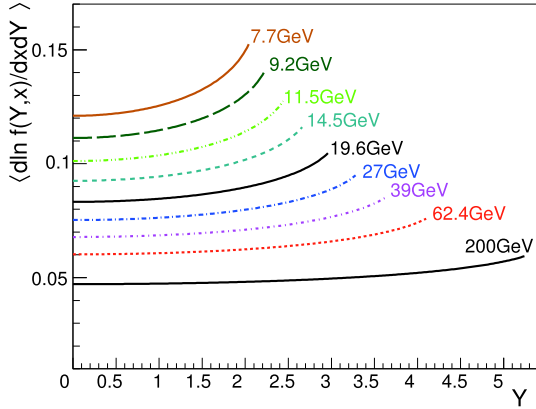


Fig. 5. (color online) Average SLM as functions of the rapidity Y in the HS model for Au+Au collisions at various collision energies. The impact parameter is set to $b = 1.2R_A$. The cutoff in Y at a collision energy is set to $0.9Y_L$.

verage SLM.

From Eq. (10), we obtain the average rapidity in the full rapidity range as

$$\langle Y \rangle = \frac{1}{Y_L} \langle Y^2 \rangle_{pp} \frac{C_1^+ - C_1^-}{C_1^+ + C_1^-}. \quad (19)$$

The numerical result of the above average rapidity is shown in Fig. 6. The result for $\langle Y \rangle$ in the WS model in the next subsection (see Fig. 10) is similar to the result of Eq. (19) or Fig. 6, except in the boundary region. Comparison with the result of Ref. [25] is also made in Fig. 10.

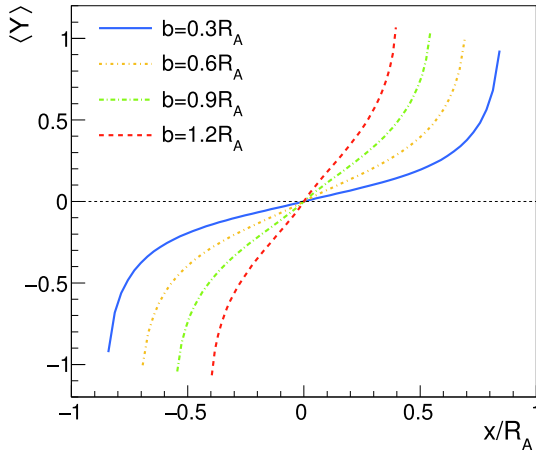


Fig. 6. (color online) Average rapidity in the full rapidity range for Au+Au collisions at $\sqrt{s_{NN}} = 200$ GeV as functions of x from Eq. (19) in the HS model.

B. Woods-Saxon nuclear density distribution

In this subsection, we choose a more realistic nuclear density distribution, the WS distribution, defined as

$$f_{WS}(\mathbf{r}) = \frac{C_0}{\exp[(r - R_A)/a] + 1}, \quad (20)$$

where $r = |\mathbf{r}|$, $a = 0.54$ fm, and C_0 is a normalization constant to make the volume integral of $f_{WS}(\mathbf{r})$ equal to the number of nucleons in the nucleus,

$$C_0 = \frac{A}{4\pi} \left[\int_0^\infty dr r^2 \frac{1}{\exp[(r - R_A)/a] + 1} \right]^{-1}. \quad (21)$$

For Au-197 nuclei, we have $R_A \approx 6.98$ fm and $C_0 \approx A/(4\pi)/120.2 \approx 0.131$ fm $^{-3}$. According to the Glauber model, the participant nucleon number density for two colliding nuclei is given by

$$\rho_{WS}^{A,B}(\mathbf{r}_T \mp \mathbf{b}/2) = f_{WS}^{A,B}(\mathbf{r}_T \mp \mathbf{b}/2) \times \left\{ 1 - \exp \left[-\sigma_{NN} \int dz f_{WS}^{B,A}(\mathbf{r}_T \pm \mathbf{b}/2) \right] \right\}, \quad (22)$$

where σ_{NN} can be taken as the inelastic pp collision cross-section.

We consider collisions of two identical nuclei. With the WS distribution in Eq. (20), we can calculate $f(Y, x)$ in Eq. (7). From Eq. (5), the thickness function becomes

$$T_A(\mathbf{r}_T \pm \mathbf{b}/2) = \int_{-\infty}^{\infty} dz \rho_{WS}^A(\mathbf{r}_T \pm \mathbf{b}/2) = \int_{-\infty}^{\infty} dz f_{WS}(\mathbf{r}_T \pm \mathbf{b}/2) \times \left\{ 1 - \exp \left[-\sigma_{NN} \int dz f_{WS}(\mathbf{r}_T \mp \mathbf{b}/2) \right] \right\}. \quad (23)$$

Substituting Eq. (23) into Eqs. (4) and (6), we obtain the hadron distribution $dN_{AA}/(dx dy dY)$ in the xy plane and $dN_{AA}/(dx dY)$ by an integration over y , respectively. The numerical results for $dN_{AA}/(dx dy dY)$ and $dN_{AA}/(dx dY)$ are shown in Figs. 7 and 8, respectively for different rapidity values in Au+Au collisions at 200 GeV with $b = 1.2R_A$. Similar to the results of the HS model in Figs. 3 and 4, in the forward/backward rapidity region, the hadron distributions are tilted toward the positive/negative x . However, different from the results of the HS model, the hadron distributions in the WS model are smooth at the edge of the overlapping region.

In Fig. 9, we show numerical results for the average SLM, applying Eq. (14) to the WS model. We choose $b = 1.2R_A$ in Au+Au collisions at different collision energies. We choose σ_{NN} as the inelastic proton-proton cross-section determined by the global fit of the experimental data [34], whose values are listed in Table 2. Also shown

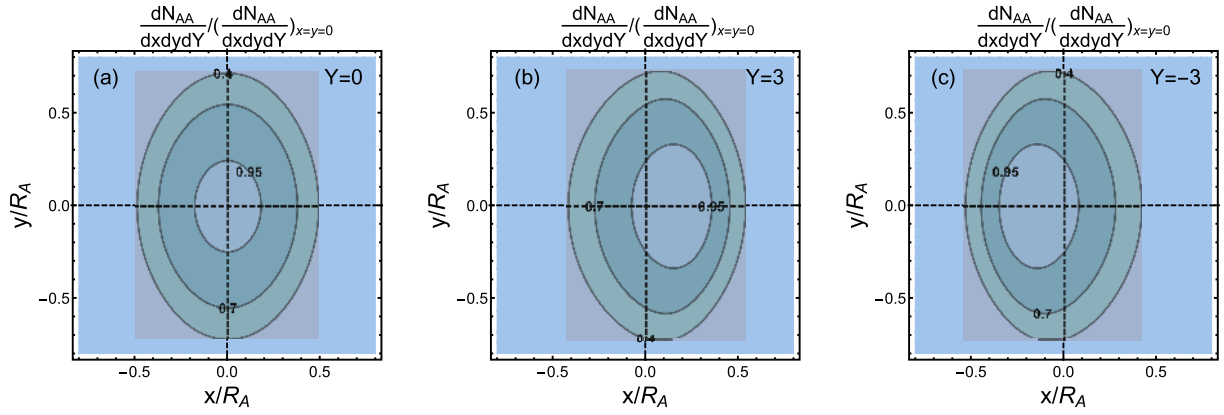


Fig. 7. (color online) Hadron distributions (contour plot) in the WS model in the transverse plane for Au+Au collisions at $\sqrt{s_{NN}} = 200$ GeV and $b = 1.2R_A$. The number on the contour line denotes the value on the line normalized by that at the origin. The rapidity values are chosen to be (a) $Y = 0$ (central), (b) $Y = 3$ (forward), and (c) $Y = -3$ (backward).

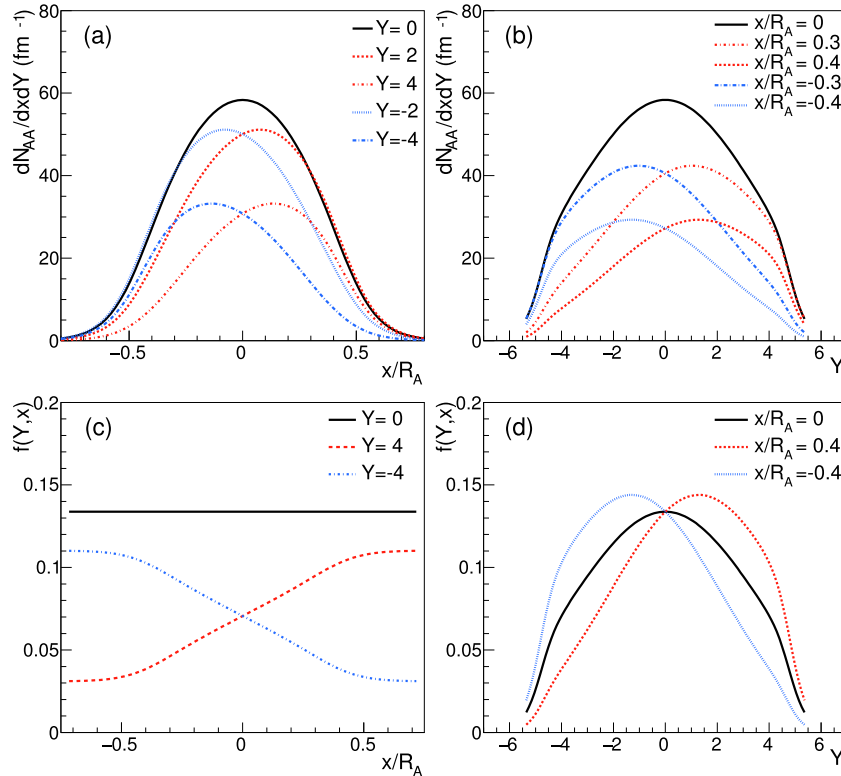


Fig. 8. (color online) Hadron distributions in the WS model in Au+Au collisions at $\sqrt{s_{NN}} = 200$ GeV as functions of (a) the in-plane position x at different rapidity values and as functions of (b) the rapidity Y at different values of x . The impact parameter is set to $b = 1.2R_A$. (c) The normalized distribution $f(Y, x)$ as functions of x at different Y . (d) The normalized distribution $f(Y, x)$ corresponding to (b). The definition of $f(Y, x)$ is given in Eq. (7).

in Table 2 are the values of the average SLM at $Y = 0$ in Au+Au collisions with the HS and WS distributions.

Similar to the results of the HS model, the average SLM at $Y = 0$ increases with decreasing collision energies, and it is a slowly increasing function of Y . There are also some differences between the WS and HS results. First, because of the smooth function in the WS model at the edge of the nucleus, the rapidity dependence of the average SLM in the WS model is slightly weaker than

that in the HS model. Second, in addition to the explicit collision energy dependence of Y_L , σ_{NN} also depends on the collision energy and enters the thickness function via Eq. (22); therefore, the increase in the average SLM at $Y = 0$ in the WS model with decreasing collision energy is slightly slower than in the HS model.

The numerical result for the average rapidity in the full rapidity range from Eq. (10) is shown in Fig. 10. In the figure, the result of Fig. 5 at $b = 0.6R_A$ in Ref. [25] is

Table 2. Inelastic nucleon-nucleon cross-section σ_{NN} at different collisions energies (first two rows). The numerical results of the average SLM at $Y = 0$ in Au+Au collisions at different collisions energies (last two rows). The impact parameter is set to $b = 1.2R_A$ corresponding to 20%-50% centrality in experiments.

| $\sqrt{s_{NN}}/\text{GeV}$ | 200 | 62.4 | 54.4 | 39 | 27 | 19.6 | 14.5 | 11.5 | 9.2 | 7.7 |
|--|--------|--------|--------|--------|--------|--------|--------|--------|--------|--------|
| σ_{NN}/mb | 42.0 | 36.3 | 35.2 | 33.6 | 32.8 | 32.3 | 31.8 | 31.4 | 30.9 | 30.6 |
| $\langle \frac{d \ln f(Y,x)}{dY dx} \rangle_{x,\text{HS}}$ | 0.0471 | 0.0602 | 0.0622 | 0.0678 | 0.0753 | 0.0833 | 0.0925 | 0.101 | 0.111 | 0.121 |
| $\langle \frac{d \ln f(Y,x)}{dY dx} \rangle_{x,\text{WS}}$ | 0.0374 | 0.0460 | 0.0472 | 0.0507 | 0.0558 | 0.0614 | 0.0678 | 0.0739 | 0.0809 | 0.0876 |

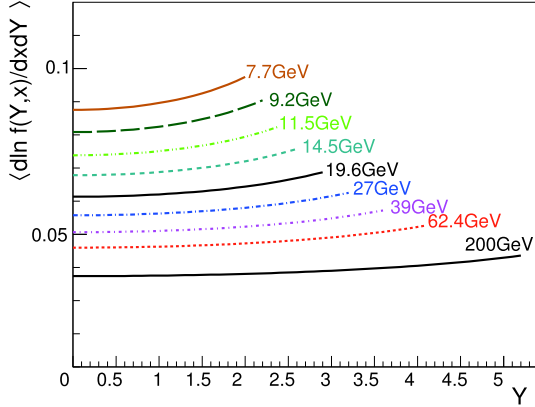


Fig. 9. (color online) Average SLM as functions of the rapidity Y in the WS model for Au+Au collisions at various collision energies. The impact parameter is set to $b = 1.2R_A$. The cutoff in Y at a collision energy is set to $0.9Y_L$.

also shown for comparison. The strong fluctuations at the edge in the simulation result of Ref. [25] are due to the small number of nucleons in the boundary region. The difference between Fig. 10 with the WS distribution and Fig. 6 with the HS distribution is that the edge of the overlapping region of two nuclei $\langle Y \rangle$ with the WS distribution is smoothly vanishing far outside the overlapping region, but $\langle Y \rangle$ with the HS distribution is discontinuous at the boundary.

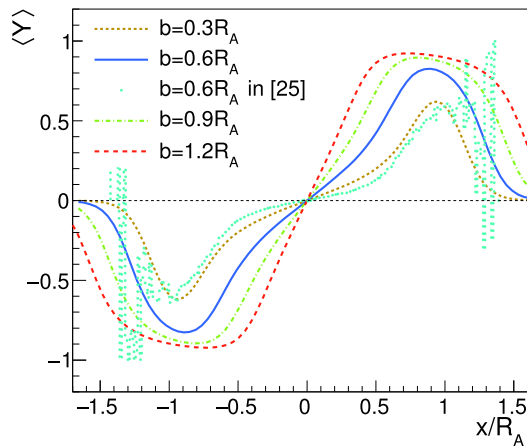


Fig. 10. (color online) Average rapidity in the full rapidity range for Au+Au collisions $\sqrt{s_{NN}} = 200$ GeV as a function of x from Eq. (10) in the WS model.

IV. POLARIZATION INDUCED BY ORBITAL ANGULAR MOMENTUM

As proposed in [25], the OAM in peripheral collisions of two nuclei can induce hadron polarization. Here, we assume that the polarization is proportional to the local OAM

$$P_q(Y) = \alpha(Y) \langle L_y \rangle = -\alpha(Y) (\Delta x)^2 \frac{\Delta_Y^2}{24} \langle p_T \rangle \left\langle \frac{d \ln f(Y,x)}{dY dx} \right\rangle_x, \quad (24)$$

where we have replaced the SLM in Eq. (13) with its average in Eq. (14), and $\alpha(Y)$ is a rapidity-dependent coefficient. The minus sign means that the polarization is along the $-y$ direction. We define a parameter

$$\kappa(Y) = \alpha(Y) (\Delta x)^2 \Delta_Y^2, \quad (25)$$

as a function of Y . Note that in principle Δx , Δ_Y , and $\langle p_T \rangle$ can also depend on Y .

The global polarization of Λ hyperons at mid-rapidity has been measured in the STAR experiment, by which the parameters in Eq. (24) can be determined. At mid-rapidity $Y = 0$, Eq. (24) becomes

$$P_q(Y=0) = -\frac{1}{24} \kappa_0 \langle p_T \rangle \left\langle \frac{d \ln f(Y,x)}{dY dx} \right\rangle_{x,Y=0}, \quad (26)$$

where we have combined three parameters into one, $\kappa_0 \equiv \kappa(Y=0)$. The average transverse momentum $\langle p_T \rangle$ as a function of the rapidity and collision energy can be fitted using available data for Kaons; see Appendix C. Results of the average SLM at $Y = 0$ are already shown in Table 2.

As our first option, we assume that the parameter κ_0 is a constant of the collision energy, whose value is chosen to describe via Eq. (26) the polarization data in the energy range of 7.7-62.4 GeV. The results are shown in the left panel of Fig. 11. We see that the collision energy dependence of $P_q(Y=0)$ in HS with $\kappa_0 = 6.4$ and that in WS with $\kappa_0 = 8.4$ are roughly consistent with the polarization data in the energy range of 7.7-62.4 GeV, but not consistent with the data at 200 GeV. Interestingly, we

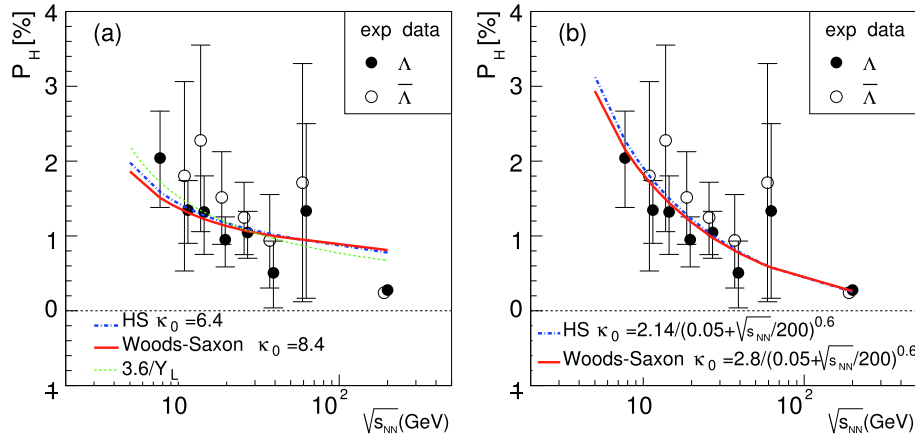


Fig. 11. (color online) Global polarization of Λ and $\bar{\Lambda}$ at mid-rapidity in the HS and WS models in Au+Au collisions at different collision energies. The impact parameter is set to $b = 1.2R_A$, corresponding to a centrality of 20%-50%. The STAR data are represented by the solid (Λ) and open ($\bar{\Lambda}$) circles [13, 14]. (a) κ_0 is a constant of the collision energy. (b) κ_0 depends on the collision energy.

find that the energy dependence of our results in both the HS and WS models can be well fitted by $1/Y_L$ behavior, but as in both the HS and WS models, it fails to describe the data at 200 GeV. The reason why we look at such a behavior is because there is a prefactor $1/Y_L$ in the SLM, as shown in Eq. (37), while the rest of the SLM depends weakly on collision energies. As our second option, we use the energy-dependent κ_0 to fit the data in the energy range of 7.7-62.4 GeV, including 200 GeV. The results are shown in the right panel of Fig. 11. We will choose the energy-dependent κ_0 to calculate the rapidity dependence of the global polarization of Λ hyperons.

As a test of the model, we calculate the global Λ polarization at 200 GeV as a function of centralities and compare it with the STAR data [14]. We use the value of κ_0 at 200 GeV and a centrality of 20%-50%. The values of $\langle p_T \rangle$ also depend on the centralities and are determined by Table 7 in Ref. [35]. The correspondence between the impact parameter and the centrality is given by Table 2 in Ref. [35]. Then, the main source of the centrality dependence of the global Λ polarization is the average SLM. The calculated result is shown in Fig. 12. We see that the theoretical result increases with the centralities and agrees with the data very well. We also see that in most central collisions, the global polarization vanishes, which indicates a vanishing SLM [1].

Once the values of κ_0 are constrained by the polarization data at mid-rapidity, we can predict the polarization of Λ hyperons at a larger rapidity. In our prediction, we use the WS model and the energy-dependent κ_0 , as determined in the right panel of Fig. 11. Because we do not know the exact rapidity dependence of $\kappa(Y)$ and $\langle p_T \rangle$, we will consider four cases and make corresponding predictions for the rapidity dependence of the global polarization:

(a) Both $\kappa(Y) = \kappa_0$ and $\langle p_T \rangle$ are taken to be constants in rapidity. Therefore, the rapidity dependence of the

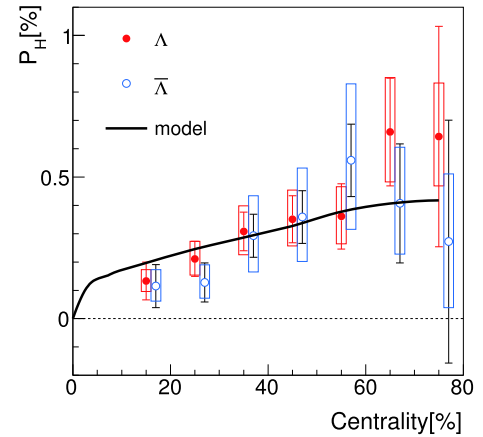


Fig. 12. (color online) Global Λ polarization as a function of centralities in comparison with the STAR data [14].

global polarization comes solely from the average SLM. This result is shown in Fig. 13(a). We see that the polarization increases slightly with Y at each collision energy. The positive slope in rapidity (the increase rate of the polarization per unit rapidity) decreases with the collision energy.

(b) Only $\kappa(Y) = \kappa_0$ is assumed to be constant in rapidity, while $\langle p_T \rangle$ depends on the rapidity. The mid-rapidity values of $\langle p_T \rangle$ are taken from the kaon data in Au+Au collisions in the collision energy range of 7.7-200 GeV [35, 36]. The rapidity dependence of $\langle p_T \rangle$ is given by fitting the kaon data in Au+Au collisions at 62.4 GeV and 200 GeV [37, 38]. For the explicit form of $\langle p_T \rangle$ as functions of rapidity and collision energy, see Appendix C. The result is shown in Fig. 13(b). We see that the polarization decreases with Y for each collision energy. At lower energies, the decreasing slope (the absolute value of the slope) is larger than that at higher energies. At 200 GeV, the polarization is almost a constant of rapidity.

(c) A rapidity constant $\langle p_T \rangle$ is adopted, which takes its value at mid-rapidity at each energy, but the rapidity

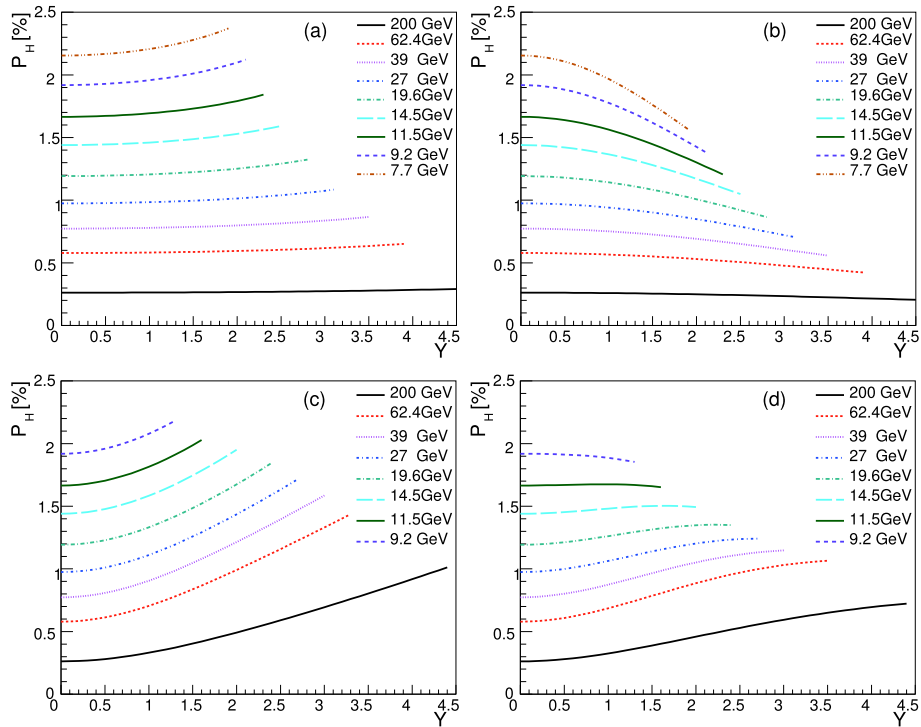


Fig. 13. (color online) Global polarization of Λ (including $\bar{\Lambda}$) in the WS model as functions of rapidity in Au+Au collisions at different collision energies. We use the collision energy-dependent κ_0 , as determined in the right panel of Fig. 11. The impact parameter is set to $b = 1.2R_A$, corresponding to a centrality of 20%-50%. The results in cases (a), (b), (c), and (d) are presented in panels (a), (b), (c), and (d) respectively.

dependence of $\kappa(Y)$ is assumed to take the form in Eq. (42). The result is shown in Fig. 13(c), where the polarization increases with rapidity. As the collision energy decreases, the slope increases. This increasing trend is stronger than that in cases (a) and (d) for the same collision energy.

(d) Both $\kappa(Y)$ and $\langle p_T \rangle$ depend on the rapidity. The rapidity dependence of $\langle p_T \rangle$ is the same as that in case (b), while the rapidity dependence of $\kappa(Y)$ is the same as that in case (c). The result is shown in Fig. 13(d). At high energies, the polarizations increase weakly with rapidity, while they are almost constants of rapidity at low energies. The result of this case is our main prediction.

Note that the form of $\kappa(Y)$ in Eq. (42) used in cases (c) and (d) is valid for $\mu_B \lesssim 0.45$ GeV; however, it is beyond such a μ_B limit at 7.7 GeV. Therefore, the curves of 7.7 GeV in Figs. 13(c,d) are not shown because they are not reliable.

V. SUMMARY

We propose a geometric model for hadron polarization in heavy ion collisions, with an emphasis on the rapidity dependence. This model is based on the model of Brodsky, Gunion, and Kuhn as well as the Bjorken scaling model [25]. The starting point is the hadron rapidity distribution $d^3N_{AA}/d^2r_T dY$ as a function of the transverse

position r_T in the overlapping region of colliding nuclei and the rapidity Y . We use the hard sphere and Woods-Saxon models for the nuclear density distribution, from which the thickness function is obtained. The rapidity distribution $d^3N_{AA}/dx dY$ depending on the in-plane position x in the overlapping region can be derived from $d^3N_{AA}/d^2r_T dY$ by integration over the out-plane position y . The average rapidity of hadrons can be obtained from the normalized distribution $d^3N_{AA}/dx dY$ or $f(Y, x)$. The collective longitudinal momentum $\langle p_z \rangle$ is proportional to $d \ln f(Y, x)/dY$. Then, the average local orbital angular momentum $\langle L_y \rangle$ is proportional to the average shear of longitudinal momentum over x , which is a function of Y . The hadron polarization is assumed to be proportional to $\alpha(Y) \langle L_y \rangle = \kappa(Y) \langle p_T \rangle \langle d \ln f(Y, x)/dY dx \rangle_{x, Y=0}$, where $\alpha(Y)$ and $\kappa(Y)$ are unknown rapidity functions characterizing transfer coefficients from the orbital angular momentum in the initial state to the hadron polarization in the final state. We make an ansatz for $\kappa(Y)$ based on the similarity in hadron production between the case at forward rapidity and higher collision energy and that at central rapidity and lower collision energy. While the similarity is true for hadron production, it needs to be tested for hadron polarization by experiments. The parameter κ at mid-rapidity can be constrained by the polarization data of Λ and $\bar{\Lambda}$. The rapidity dependence of $\langle p_T \rangle$ is obtained by fitting the data of kaons obtained by the BRAHMS and STAR

collaborations. Finally, we make predictions for the rapidity dependence of the hadron polarization in the collision energy range of 7.7-200 GeV. These predictions can be tested by beam-energy-scan experiments at the Relativistic Heavy Ion Collider of Brookhaven National Lab.

ACKNOWLEDGEMENTS

The authors thank C.M. Ko and J.Y. Jia for the insightful discussions.

APPENDIX A: DERIVATION OF SLM FOR HARD SPHERE DISTRIBUTION

In this appendix, we will derive the SLM $d \ln f(Y, x) /$

$dY dx$ in the HS model for the nuclear density distribution from Eqs. (17) and (18). The definitions of C_1^\pm and C_2^\pm are

$$C_1^\pm = \int_0^{y_m} dy \left[R_A^2 - (x \mp b/2)^2 - y^2 \right]^{1/2}, \quad (\text{A1})$$

$$C_2^\pm = \int_0^{y_m} dy \left[R_A^2 - (x \mp b/2)^2 - y^2 \right]^{-1/2}, \quad (\text{A2})$$

where y_m is the maximum of y at a fixed x

$$y_m = \left[R_A^2 - (|x| + b/2)^2 \right]^{1/2}. \quad (\text{A3})$$

The analytical expressions of C_1^\pm are

$$C_1^+(x) = \begin{cases} \frac{\pi}{4} \left[R_A^2 - \left(x - \frac{b}{2} \right)^2 \right], & -(R_A - \frac{b}{2}) < x \leq 0 \\ \frac{1}{2} \sqrt{R_A^2 - \left(x + \frac{b}{2} \right)^2} \sqrt{2bx} + I_-(x), & 0 < x < R_A - \frac{b}{2} \end{cases} \quad (\text{A4})$$

$$C_1^-(x) = \begin{cases} \frac{\pi}{4} \left[R_A^2 - \left(x + \frac{b}{2} \right)^2 \right], & 0 \leq x < R_A - \frac{b}{2} \\ \frac{1}{2} \sqrt{R_A^2 - \left(x - \frac{b}{2} \right)^2} \sqrt{-2bx} + I_+(x), & -(R_A - \frac{b}{2}) < x < 0 \end{cases} \quad (\text{A5})$$

where the function $I_\pm(x)$ is defined as

$$I_\pm(x) = \frac{1}{2} \left[R_A^2 - (x \pm b/2)^2 \right] \arctan \frac{\sqrt{R_A^2 - (x \mp b/2)^2}}{\sqrt{\mp 2bx}}. \quad (\text{A6})$$

The analytical expressions of C_2^\pm are

$$C_2^+(x) = \begin{cases} \arctan \frac{\sqrt{R_A^2 - (x + b/2)^2}}{\sqrt{2bx}}, & 0 < x < R_A - b/2 \\ \frac{\pi}{2}, & -(R_A - b/2) < x \leq 0 \end{cases} \quad (\text{A7})$$

$$C_2^-(x) = \begin{cases} \frac{\pi}{2}, & 0 \leq x < R_A - b/2 \\ \arctan \frac{\sqrt{R_A^2 - (x - b/2)^2}}{\sqrt{-2bx}}, & -(R_A - b/2) < x < 0 \end{cases} \quad (\text{A8})$$

In terms of C_1^\pm and C_2^\pm , we obtain the derivative of $\ln f(Y, x)$ with respect to Y as

$$\frac{d \ln f(Y, x)}{dY} = \frac{d \ln(dN_{pp}/dY)}{dY} + \frac{1}{Y} - \frac{1}{Y} \left[1 + \frac{Y}{Y_L} \cdot \frac{C_1^+ - C_1^-}{C_1^+ + C_1^-} \right]^{-1}, \quad (\text{A9})$$

after which the derivative of $d \ln f(Y, x) / dY$ with respect to x is

$$\frac{d \ln f(Y, x)}{dY dx} = \frac{1}{Y_L} \left[1 + \frac{Y}{Y_L} \cdot \frac{C_1^+ - C_1^-}{C_1^+ + C_1^-} \right]^{-2} \left\{ -\frac{x(C_2^+ - C_2^-) - (b/2)(C_2^+ + C_2^-)}{(C_1^+ + C_1^-)} + \frac{(C_1^+ - C_1^-) [x(C_2^+ + C_2^-) - (b/2)(C_2^+ - C_2^-)]}{(C_1^+ + C_1^-)^2} - 2 \sqrt{2b|x|} (|x| + b/2) \sqrt{R_A^2 - (|x| + b/2)^2} \frac{C_1^+ \theta(-x) + C_1^- \theta(x)}{(C_1^+ + C_1^-)^2} \right\}, \quad (\text{A10})$$

where we have used

$$\frac{d}{dx} \int_0^{a(x)} dy b(x, y) = \int_0^{a(x)} dy \frac{\partial b(x, y)}{\partial x} + b(x, a(x)) \frac{da(x)}{dx}. \quad (\text{A11})$$

APPENDIX B: RAPIDITY DEPENDENCE OF $\kappa(Y)$

There is a similarity in hadron production between the case at forward rapidity and higher collision energy and that at central rapidity and lower collision energy. Thus, the baryon number density or baryon chemical potential is the relevant physical quantity in both cases. Therefore, if we neglect the system size effect, we can make an ansatz for $\kappa(Y)$ based on this correspondence.

By fitting the data in Fig. 8(b), we find the following energy behavior for $\kappa_0 \equiv \kappa(Y=0)$,

$$\kappa_0 = \frac{2.8}{(0.05 + \sqrt{s_{NN}}/200)^{0.6}}. \quad (\text{B1})$$

The collision energy dependence of the baryon chemical potential at mid-rapidity can be given by [39]

$$\mu_B(0) \equiv \mu_B(Y=0) = \frac{1.3075}{1 + 0.288 \sqrt{s_{NN}}} \text{ GeV}. \quad (\text{B2})$$

We can solve $\sqrt{s_{NN}}$ as a function of $\mu_B^{(0)}$ and obtain

$$\kappa_0 = \frac{2.8}{[0.05 + (1.3075/\mu_B(0) - 1)/57.6]^{0.6}}, \quad (\text{B3})$$

in the range of $\mu_B^{(0)} \lesssim 0.45$ GeV, i.e., in the collision energy range of 7.7-200 GeV. We can generalize the above expression to other rapidity values as

$$\kappa(Y) = \frac{2.8}{[0.05 + (1.3075/\mu_B(Y) - 1)/57.6]^{0.6}}, \quad (\text{B4})$$

by taking the following parameterization of $\mu_B(Y)$ [40]

$$\mu_B(Y) = \mu_B(0) + (0.09527 - 0.01594 \log \sqrt{s_{NN}}) Y^2. \quad (\text{B5})$$

APPENDIX C: RAPIDITY DEPENDENCE OF $\langle p_T \rangle$

The average transverse momentum $\langle p_T \rangle$ also has rapidity dependence. The $\langle p_T \rangle$ data for kaons at different rapidities are measured by the BRAHMS collaboration at 200 and 62 GeV [37, 38], which can be parameterized as

$$\langle p_T \rangle_Y \approx \langle p_T \rangle_0 \exp\left(-\frac{Y^2}{2Y_L^2}\right), \quad (\text{C1})$$

where $\langle p_T \rangle_0 \equiv \langle p_T \rangle_{Y=0}$ denotes the average transverse momentum at mid-rapidity; see Fig. C1. Here, $\langle p_T \rangle_0$ also depends on the collision energy and can be parameterized as

$$\langle p_T \rangle_0 = 0.41634 + 0.030644 s_{NN}^{1/4} - 0.0011547 s_{NN}^{1/2}, \quad (\text{C2})$$

following STAR data for kaons at $\sqrt{s_{NN}} = 7.7$ -200 GeV [35, 36], where the unit of $\langle p_T \rangle_0$ is GeV and $s_{NN}^{1/2}$ takes the dimensionless value of the collision energy in GeV; see Fig. C2.

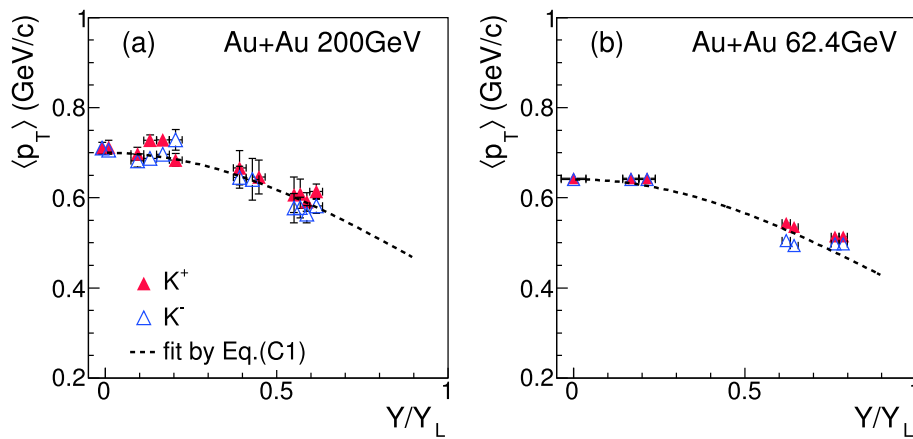


Fig. C1. (color online) Average transverse momentum $\langle p_T \rangle$ for kaons as functions of rapidity in central Au+Au collisions.

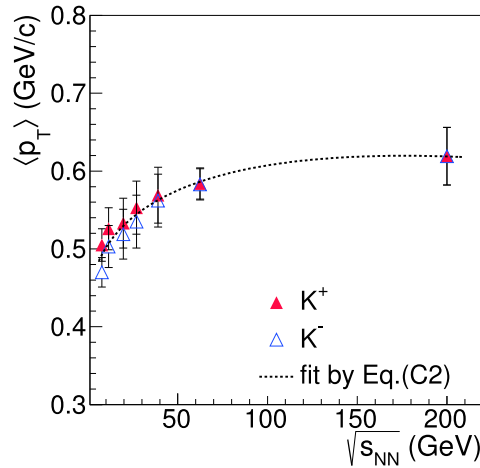


Fig. C2. (color online) Average transverse momentum at mid-rapidity $\langle p_T \rangle_0$ for kaons as functions of collision energies in semi-central (40%-50%) Au+Au collisions.

References

- [1] Z. T. Liang and X. N. Wang, *Phys. Rev. Lett.* **94**, 102301 (2005)
- [2] Z. T. Liang and X. N. Wang, *Phys. Lett. B* **629**, 20 (2005)
- [3] S. A. Voloshin, (2004) nucl-th/0410089
- [4] B. Betz, M. Gyulassy, and G. Torrieri, *Phys. Rev. C* **76**, 044901 (2007)
- [5] F. Becattini, F. Piccinini, and J. Rizzo, *Phys. Rev. C* **77**, 024906 (2008)
- [6] F. Becattini, G. Inghirami, V. Rolando *et al.*, *Eur. Phys. J. C* **75**(9), 406 (2015)
- [7] L.G. Pang, H. Petersen, Q. Wang *et al.*, *Phys. Rev. Lett.* **117**(19), 192301 (2016)
- [8] W. T. Deng and X. G. Huang, *Phys. Rev. C* **93**(6), 064907 (2016)
- [9] Y. Jiang, Z. W. Lin, and J. Liao, *Phys. Rev. C* **94**(4), 044910 (2016)
- [10] F. Becattini, V. Chandra, L. Del Zanna *et al.*, *Annals Phys.* **338**, 32 (2013)
- [11] R.H. Fang, L.G. Pang, Q. Wang *et al.*, *Phys. Rev. C* **94**(2), 024904 (2016)
- [12] Q. Wang, *Nucl. Phys. A* **967**, 225 (2017)
- [13] L. Adamczyk *et al.* (STAR Collaboration), *Nature* **548**, 62 (2017)
- [14] J. Adam, *et al.* (STAR Collaboration), *Phys. Rev. C* **98**, 014910 (2018)
- [15] M. Baznat, K. Gudima, A. Sorin *et al.*, *Phys. Rev. C* **88**(6), 061901 (2013)
- [16] L. P. Csernai, V. K. Magas, and D. J. Wang, *Phys. Rev. C* **87**(3), 034906 (2013)
- [17] L. P. Csernai, D. J. Wang, M. Bleicher *et al.*, *Phys. Rev. C* **90**(2), 021904 (2014)
- [18] O. Teryaev and R. Usubov, *Phys. Rev. C* **92**(1), 014906 (2015)
- [19] Yu. B. Ivanov and A. A. Soldatov, *Phys. Rev. C* **95**(5), 054915 (2017)
- [20] H. Li, L. G. Pang, Q. Wang *et al.*, *Phys. Rev. C* **96**(5), 054908 (2017)
- [21] D. X. Wei, W. T. Deng, and X. G. Huang, *Phys. Rev. C* **99**(1), 014905 (2019)
- [22] I. Karpenko and F. Becattini, *Eur. Phys. J. C* **77**(4), 213 (2017)
- [23] Y. Xie, D. Wang, and L. P. Csernai, *Phys. Rev. C* **95**(3), 031901 (2017)
- [24] Y. Sun and C. M. Ko, *Phys. Rev. C* **96**(2), 024906 (2017)
- [25] J. H. Gao, S. W. Chen, W. T. Deng *et al.*, *Phys. Rev. C* **77**, 044902 (2008)
- [26] S. J. Brodsky, J. F. Gunion, and J. H. Kuhn, *Phys. Rev. Lett.* **39**, 1120 (1977)
- [27] J. Bjorken, *Phys. Rev. D* **27**, 140 (1983)
- [28] R. D. Woods and D. S. Saxon, *Phys. Rev.* **95**, 577 (1954)
- [29] T. Sjostrand, S. Ask, J. R. Christiansen *et al.*, *Comput. Phys. Commun.* **191**, 159 (2015)
- [30] B. Andersson, G. Gustafson, and B. Nilsson-Almqvist, *Nucl. Phys. B* **281**, 289 (1987)
- [31] X. N. Wang and M. Gyulassy, *Phys. Rev. D* **44**, 3501 (1991)
- [32] M. Gyulassy and X. N. Wang, *Comput. Phys. Commun.* **83**, 307 (1994)
- [33] A. Adil and M. Gyulassy, *Phys. Rev. C* **72**, 034907 (2005)
- [34] K. A. Olive *et al.* (Particle Data Group Collaboration), *Chin. Phys. C* **38**, 090001 (2014)
- [35] B. I. Abelev *et al.* (STAR Collaboration), *Phys. Rev. C* **79**, 034909 (2009)
- [36] L. Adamczyk *et al.* (STAR Collaboration), *Phys. Rev. C* **96**(4), 044904 (2017)
- [37] I. C. Arsene *et al.* (BRAHMS Collaboration), *Phys. Lett. B* **687**, 36 (2010)
- [38] I. G. Bearden *et al.* (BRAHMS Collaboration), *Phys. Rev. Lett.* **94**, 162301 (2005)
- [39] A. Andronic, P. Braun-Munzinger, K. Redlich *et al.*, *Nature* **561**(7723), 321 (2018)
- [40] F. Becattini, J. Cleymans, and J. Strumpfer, *PoS CPOD07*, 012 (2007)